

# Perpendicular magnetic anisotropy in nanoclusters caused by surface segregation and shape

Stefan Heinrichs<sup>1</sup>, Wolfgang Dieterich<sup>1</sup> and Philipp Maass<sup>2</sup>

<sup>1</sup>*Fachbereich Physik, Universität Konstanz, 78457 Konstanz, Germany*

<sup>2</sup>*Institut für Physik, Technische Universität Ilmenau, 98684 Ilmenau, Germany*

(Dated: September 13, 2005)

The growth of binary alloy clusters on a weakly interacting substrate through codeposition of two atomic species is studied by kinetic Monte Carlo simulation. Our model describes salient features of CoPt<sub>3</sub>-nanoclusters, as obtained recently by the molecular-beam epitaxy technique. The clusters display perpendicular magnetic anisotropy (PMA) in a temperature window of growth favorable for applications. This temperature window is found to arise from the interplay of Pt surface segregation and aspect ratio for cluster shapes. Conclusions are drawn how to optimize growth parameters with respect to PMA.

PACS numbers: 81.15.Aa, 68.55.Ac, 75.75.+a

Growth of frozen-in metastable structures by molecular beam epitaxy (MBE) opens a wide field for producing materials with novel properties. In most cases, the growth conditions require a description based on far-from-equilibrium kinetics. Especially interesting are multicomponent systems or systems with internal degrees of freedom (magnetic or electrical moments) that couple to the atomic structure. A rich variety of material properties is then expected to emerge from the elementary processes of deposition, adatom diffusion, surface nucleation, as well as from structural and compositional changes of islands, from surface segregation or magnetic ordering.

MBE growth of binary magnetic alloy thin films and nanoclusters has recently attracted much attention in the search for materials with an easy magnetic axis perpendicular to the substrate [1, 2]. Such perpendicular magnetic anisotropy (PMA) can be utilized to increase magnetic storage densities. In thin magnetic films the dipolar form anisotropy favors alignment of the magnetic moments parallel to the substrate. To achieve PMA in thin films, the dipolar form anisotropy has to be overcome by effects based on local atomic arrangements.

The system Co/Pt is particularly intriguing, as PMA could be obtained in different ways: *(i)* In Co/Pt multilayers the magnetic moments of Co-atoms preferentially align along the interfacial Co-Pt bonds and PMA is found in magnetic X-ray circular dichroism studies to originate at the interfaces [3]. *(ii)* In disordered films with CoPt<sub>3</sub>-stoichiometry grown in [111] direction, PMA is found in a temperature window 500 K <  $T$  < 820 K [4]. XAFS [5] and EXAFS [6] experiments show the preferential occurrence of Co/Pt bonds out of plane. These were associated with surface-induced formation of flat Co-rich domains, as suggested by the increase of Curie temperatures with respect to those for disordered bulk Co/Pt-alloys [4]. *(iii)* In CoPt<sub>3</sub> nanoclusters with 300 to 1000 atoms, grown by codeposition of Co and Pt on WSe<sub>2</sub> van-der-Waals surfaces, PMA is observed near ambient growth temperatures [7], favorable for applications. The

underlying structural anisotropy, however, is not understood so far.

In fact, the occurrence of PMA in nanoclusters is surprising in view of the kinetic limitations induced by comparatively low growth temperatures. Several mechanisms can be envisaged in principle. One possibility might be a bulk anisotropy arising from formation of Co-rich domains in the bulk, similar to [4]. Alternatively, PMA connected with the surface could be induced by Pt surface segregation. A further question concerns the interplay between L1<sub>2</sub> ordering and PMA.

In this Letter we investigate non-equilibrium structures that emerge from the combined effects of deposition, surface diffusion and ordering phenomena in a model for binary alloy growth. We find that surface segregation together with cluster shape formation leads to a structural anisotropy that induces PMA. There is no evidence for significant bulk contributions facilitating PMA. In order to account for the experimentally observed phenomena, exchange processes during growth between low-coordinated atoms at the cluster surface have to be included.

To demonstrate these mechanisms, we analyze a model based on nearest neighbor interactions  $V_{AA}$ ,  $V_{AB}$ ,  $V_{BB}$  between atomic species A and B, which are adjusted to the CoPt<sub>3</sub> system (A=Co, B=Pt). The parameter  $J = (V_{AA} + V_{BB} - 2V_{AB})/4$  fixes the bulk order-disorder temperature  $T_0 = 1.83J/k_B$  [8]. With  $T_0 = 958$  K [9] we take  $k_B T_0/1.83 = 45$  meV as our energy unit. The parameter  $h = V_{BB} - V_{AA}$  controls the surface segregation of B atoms at equilibrium. Segregation with nearly 100% Pt at the surface [10] is compatible with  $h \simeq 4$ . The parameter  $V_0 = (V_{AB} + V_{BB})/2$  represents the average bond energy in the L1<sub>2</sub>-ordered crystal, and together with  $J$  and  $h$  uniquely determines the bond energies  $V_{AA}$ ,  $V_{AB}$ , and  $V_{BB}$ . Its estimation from the cohesive energy of L1<sub>2</sub> ordered CoPt<sub>3</sub>, however, would not be appropriate, because in real materials the total binding energy is not given by a sum of independent bond interactions [11].

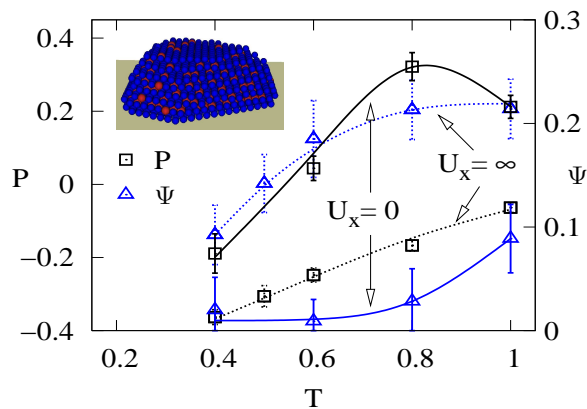


FIG. 1: (color online) Structural anisotropy  $P$  and  $L_{12}$  order parameter  $\Psi$  for clusters of size 1000 for different substrate temperatures, with  $h = 4$ . The solid (dashed) lines are a guide to the eye for exchange barriers  $U_x = 0$  ( $U_x = \infty$ ). The inset shows a typical configuration ( $U_x = 0$ ,  $T = 1$ ) before subsequent equilibration. Pt atoms are marked in blue (dark) and Co atoms in red.

Rather we note that during cluster growth the mobility is effectively restricted to the surface, so that the number of relevant bonds per atom is between 3 (for a diffusing adatom) and 7 (for an atom at an edge). Parameters for a variety of corresponding processes were calculated for Pt with DFT [12] and yield  $V_0 \simeq -5$ , which we adopt here.

Binding to the substrate surface is represented by a weak potential  $V_s = -5$  restricted to adatoms in the first layer. Compared to a Pt(111) surface with three bonds of typical strength  $V_0$ , this amounts to about 1/3 of the energy of a single Pt-Pt bond.

To model the growth of the clusters, we perform kinetic Monte-Carlo (KMC) simulations on an fcc lattice with periodic boundary conditions in the lateral directions. Compared to previous growth simulations of binary alloys with solid-on-solid models or immediate downward funneling, our program is fully three-dimensional, so that for instance diffusion on equivalent side facets is automatically equivalent to diffusion on the top terrace. A rejectionless continuous-time algorithm is implemented that generates cluster configurations with statistical weights according to the underlying master equation. The possible elementary processes are jumps of A or B atoms to vacant nearest neighbor sites and the deposition of an atom. The jump of an atom occurs with a rate  $\nu \exp(-U/k_B T) \min(1, \exp[-\Delta E/k_B T])$ , where  $\Delta E$  is the energy difference before and after the jump,  $U$  is an energy barrier and  $\nu$  an attempt frequency. Diffusion measurements of Pt on Pt(111) give  $\nu \simeq 5 \times 10^{12} \text{ s}^{-1}$  and  $U \simeq 5$ . These values are taken to be the same for all jump processes. Deposition of atoms occurs with a rate  $F = 21$  monolayers per second. The overall procedure automatically entails adatom diffusion, deposition

and re-evaporation, nucleation, step edge diffusion, and step edge barriers.

A typical cluster with  $N = 1000$  atoms is shown in the inset of Fig. 1. As in the experiments [7], side facets are of  $\{111\}$  and  $\{100\}$  type and the aspect ratio between lateral and height dimensions is about 3:1.

To quantify the long-range chemical ordering we determine the average intensity  $I$  of  $L_{12}$  superstructure peaks and normalize it with respect to surrogate structures, where the cluster shape is maintained, but the atomic configuration is changed. By occupying precisely one of the four sc-sublattices with Co atoms we obtain the intensity  $I_{\text{id}}$  for perfect  $L_{12}$  ordering, while a random occupation with the stoichiometric concentration yields  $I_{\text{ran}}$ . The order parameter is then defined as  $\Psi = (I - I_{\text{ran}})/(I_{\text{id}} - I_{\text{ran}})$ . As can be seen from Fig. 1 (triangles, dashed line),  $\Psi$  decreases by lowering the temperature due to kinetic suppression of the equilibrium state, in accordance with experiments. The extrapolated onset temperature for  $L_{12}$ -ordering, however, is much lower than in experiments. On the other hand, since the deposition rate in our simulations is larger than the experimental one, one expects a shift of calculated relative to experimental data to higher  $T$ .

This problem can be resolved by allowing for direct exchange processes between unlike neighboring atoms near the surface. As shown below, such processes also drive the Pt surface segregation which is crucial for producing PMA. In the model described before, only indirect exchange processes between two atoms can take place via intermediate states, as a result of two or more direct exchanges with vacancies. These are, however, extremely rare since realization of the intermediate states requires bond breaking steps with high activation energies. Direct exchange processes are found for Co deposited on Pt(111) over a wide temperature range 250–520 K [13, 14, 15]. They are especially frequent for low-coordinated atoms on top of terraces (with coordination 3) or at step edges (with coordinations 4 or 5).

To include these processes in the model, we allow a pair of unlike neighboring atoms to exchange sites if one of them has a coordination in the range 3 to 5 and the other one in the range 8 to 10. In addition to the difference between initial and final energies, an increased exchange barrier  $U_x + U$  has to be surmounted. Setting  $U_x = 0$  as the opposite extreme to  $U_x = \infty$  (no exchange processes), we see in Fig. 1 that the onset of  $L_{12}$ -ordering occurs near  $T \simeq 1$  (corresponding to  $T = 523 \text{ K}$ ), which is in reasonable accordance with experiments.

We now investigate the possible occurrence of a structural anisotropy that can induce PMA. Regarding magnetic properties in Co-Pt alloys, we adopt the viewpoint, suggested by the experiments discussed above [3, 4], that the crystalline magnetic anisotropy originates mainly from Co-Pt bonds, which tend to align the Co moments along the bond. PMA will therefore be

traced back to a prevalence of out-of-plane relative to in-plane Co-Pt bonds. Denoting the corresponding total numbers of bonds in a cluster of  $N$  atoms by  $n_{\perp}^{\text{CoPt}}$  and  $n_{\parallel}^{\text{CoPt}}$ , the pertinent anisotropy is introduced as  $P = (n_{\perp}^{\text{CoPt}} - n_{\parallel}^{\text{CoPt}})/N$ . PMA requires that  $P > 0$ .

In the absence of exchange processes ( $U_x = \infty$ ), simulated values for  $P$  turn out, however, to be negative as shown in Fig. 1. The reason is that the clusters are relatively flat and that surface segregation of Pt is weak. As a consequence, in a clusters' surface there exist more Co-Pt bonds in-plane than out-of-plane, while atoms in the inner part of the cluster give no contribution to  $P$ . The flat cluster shape, on the other hand, would favor PMA if strong Pt segregation, as realized at equilibrium, could build up. Indeed, when including exchange processes, the Pt segregation gets strongly enhanced and  $P$  can become positive. Actually, the cluster displayed in the inset of Fig. 1, showing pronounced Pt surface segregation, was computed with  $U_x = 0$ . As seen from the figure, for  $U_x = 0$ ,  $P$  changes sign near  $T = 0.58$  and reaches a maximum at an optimum temperature  $T_{\text{max}} \simeq 0.8$ . As in experiments [4], the subsequent decrease of  $P$  is accompanied by the onset and subsequent rise of  $L1_2$ -ordering.

To investigate the mechanisms of PMA in more detail, we show in Fig. 2a  $P$  as a function of cluster size  $N$  during growth for 4 different temperatures, and for a more realistic nonzero exchange barrier  $U_x > 0$ , which we set equal to the adatom diffusion barrier,  $U_x = U = 5$ . Except for the two lowest temperatures, where Pt segregation is not sufficiently strong,  $P$  indeed becomes positive except for very small  $N$  (not shown). Again there exists an optimal temperature  $T_{\text{max}} \simeq 1$ , where PMA is expected to be strongest. Changes of  $P$  during subsequent equilibration under zero flux are less than 15 % of the values near  $T_{\text{max}}$  and will be ignored in the following.

The existence of an optimal temperature, however, is not directly caused by  $L1_2$  ordering as one might conjecture from Fig. 1. Rather, it results from two competing effects: As shown in Fig. 2b, increasing  $T$  facilitates Pt segregation, leading to larger  $P$ . On the other hand, increasing  $T$  also drives the cluster morphology closer to an equilibrium with less flat shapes with smaller  $P$ . This effect is shown in Fig. 2c, where we plot the  $T$ -dependence of the aspect ratio, defined by the ratio  $l_{\parallel}/l_{\perp}$  of the gyration radii of cluster sizes in the direction parallel and perpendicular to the substrate. While the aspect ratio does not depend on  $U_x$ , the Pt segregation is significantly enhanced for lower  $U_x$ , see Fig. 2b. These results can explain why there exists a temperature window for PMA in experiments and why in films with tall rather than flat clusters, parallel instead of perpendicular magnetic anisotropy is favored [16].

Since the positive values of  $P$  arise due to the surface segregation of Pt, we expect  $n_{\perp}^{\text{CoPt}} - n_{\parallel}^{\text{CoPt}} \sim N^{2/3}$ , and accordingly  $P \sim N^{-1/3}$ . As shown by the solid lines in

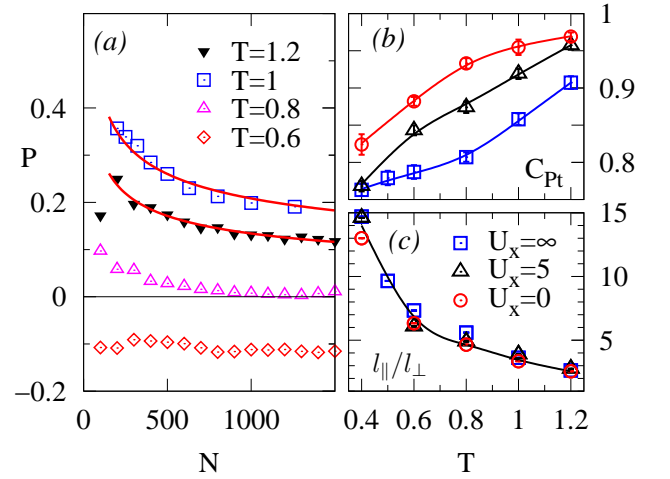


FIG. 2: (a) Anisotropy parameter  $P$  averaged over 20 clusters versus size  $N$  at different temperatures, with  $U_x = 5$ . For the two highest temperatures, the proportionality  $P \propto N^{-1/3}$  is well established, see the lines. (b) Pt concentration  $C_{\text{Pt}}$  in the outer shell of the cluster for various  $U_x$  (symbol assignment as in (c)). (c) Ratio  $l_{\parallel}/l_{\perp}$  of cluster gyration radii as a function of temperature. The line is drawn as a guide to the eye.

Fig. 2a, this behavior is well obeyed by the data sets for  $T = 1$  and  $T = 1.2$ .

We are now in the position to estimate the magnitude of the magnetic anisotropy  $E_s = E\{\vec{\mu} \text{ in plane}\} - E\{\vec{\mu} \text{ out of plane}\}$ , as expected from the data in Fig. 2.  $E\{\vec{\mu}\}$  denotes the anisotropic part of magnetic interactions as a function of Co moments  $\vec{\mu}$  for saturated magnetization. Within a simple bond picture we suppose that each Co-atom experiences a local crystalline anisotropy, which is a sum over the corresponding twelve Co- $\alpha$  bonds in the fcc-lattice with  $\alpha = \text{Co, Pt or V(vacancy)}$ , specifying the nearest neighbor occupation. Each bond with bond-vector  $\vec{\delta}$  contributes a term  $-A^\alpha (\vec{\mu} \cdot \vec{\delta}/|\vec{\mu}||\vec{\delta}|)^2$  to  $E\{\vec{\mu}\}$ , with anisotropy constants  $A^\alpha$  to be deduced from experiment. Note that for saturated magnetization a nearest-neighbor contribution to the anisotropic part of dipole-dipole interactions has exactly the same form, so that these are included already in the coefficients  $A^\alpha$ . As discussed before, the most important contribution arises from Co-Pt bonds. Anisotropy constants for Co-Pt in multi-layer systems and wedges were measured for instance with magnetic torque or the magneto-optical Kerr effect [17]. From these experiments we deduce  $A^{\text{CoPt}} = 160 \mu\text{eV}$  as a representative value. Similarly, from measurements of Co-vacuum interfaces and theoretical investigations of a freely standing Co-monolayer [17] we estimate  $A^{\text{CoV}} \simeq -67 \mu\text{eV}$ . The remaining parameter is  $A^{\text{CoCo}}$  for which we retain only the dipolar contribution. Using  $\mu^{\text{Co}} = 1.7\mu_B$  [4, 18] and  $|\vec{\delta}| = 2.72 \text{ \AA}$  in  $\text{CoPt}_3$ , this yields  $A^{\text{CoCo}} = 23 \mu\text{eV}$ .

Within this bond model it is straightforward to calculate the anisotropy energy  $E_s$ , which can be written

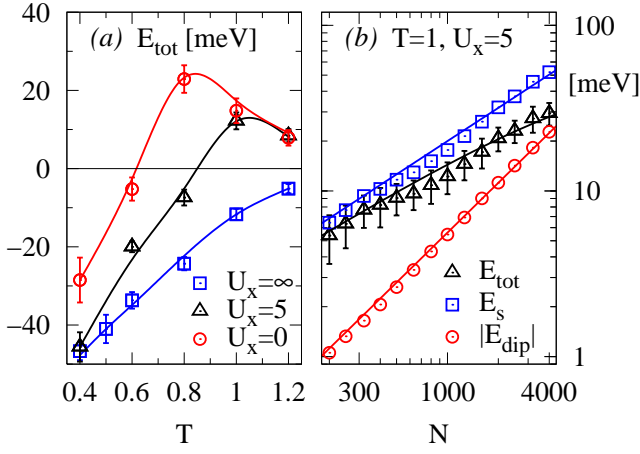


FIG. 3: (a) Total magnetic anisotropy energy  $E_{\text{tot}}$  for  $N = 10^3$  in dependence of temperature for different exchange barriers  $U_x$  for exchange processes. (b) Surface and bulk contributions  $E_s$ ,  $E_{\text{dip}}$  in dependence of cluster size  $N$ . The corresponding straight lines in the double logarithmic plot have slopes  $2/3$  and  $1$ . Data for  $E_{\text{tot}}$  are fitted according to Eq. (2).

$$E_s = \frac{1}{2} \sum_{\alpha=\text{Pt,Co}} (A^{\text{Co}\alpha} - A^{\text{CoV}})(n_{\perp}^{\text{Co}\alpha} - n_{\parallel}^{\text{CoV}}) = K_s N^{2/3} \quad (1)$$

The last equality in (1) holds on account of  $P \propto N^{-1/3}$ , see Figs. 2a and 3b. Similarly, we found that  $(n_{\perp}^{\text{CoCo}} - n_{\parallel}^{\text{CoCo}}) \propto N^{2/3}$ , but this term related to Co-Co bonds turns out to be significantly smaller than the first term in (1) in view of our estimates for  $A^{\text{Co}\alpha}$ . Altogether we find  $K_s \simeq 200 \mu\text{eV}$  at  $T = 1$  and  $U_x = 5$ .

So far we neglected contributions to the anisotropy energy from dipolar interactions between non-neighboring moments. These interactions favor an orientation of the magnetization parallel to the (111)-plane and hence give a negative bulk contribution  $E_{\text{dip}} = -K_{\text{dip}}N$  to the total anisotropy energy

$$E_{\text{tot}} = K_s N^{2/3} - K_{\text{dip}}N \quad (2)$$

From calculated cluster structures, Co magnetic moments  $1.7\mu_B$  and induced Pt magnetic moments  $0.3\mu_B$  [4, 18] we obtain  $K_{\text{dip}} \simeq 5.6 \mu\text{eV}$  at  $T = 1$ . This yields an  $E_{\text{tot}}$  that is displayed in Fig. 3a as a function of  $T$  for different  $U_x$  and  $N = 1000$ . An optimal temperature, where  $E_{\text{tot}}$  is maximum, can clearly be identified. For example, for  $U_x = 5$ ,  $T_{\text{max}} \simeq 1$ .

In Fig. 3b we show  $E_{\text{tot}}$  as a function of  $N$  for  $U_x = 5$  and  $T = 1 \simeq T_{\text{max}}$ , together with the surface and dipolar contributions  $E_s \propto N^{2/3}$  and  $E_{\text{dip}} \propto N$ . The solid line for  $E_{\text{tot}}$  represents Eq. (2), which predicts an optimal cluster size  $N_{\text{opt}} \simeq 13500$  with maximum  $E_{\text{tot}}$ . The PMA is expected to disappear for  $N > N_c \simeq 5 \cdot 10^4$ .

In summary, by simulating the fully three-dimensional kinetics of binary alloy cluster growth, we have shown

how PMA can result from the combined effect of surface segregation and flat cluster morphologies. The interplay between segregation and aspect ratio of cluster shapes explains the occurrence of a temperature window for PMA. The effect discussed here primarily relies on surface contributions and favors PMA, in contrast to the dipolar form anisotropy. Stronger segregation (e.g. due to lower exchange barriers) as well as smaller adsorbate-substrate and adsorbate-vacuum surface tensions (leading to flatter shapes) should broaden the temperature window and may guide the search for optimized materials. We expect that for  $T \simeq T_{\text{max}}$  there exists an optimal cluster size  $N_{\text{opt}}$  for PMA and a critical cluster size  $N_c = (3/2)^3 N_{\text{opt}}$ , above which PMA disappears. It should be interesting to test these predictions in experiments.

We thank M. Albrecht, M. Maret, J. Schäfer and G. Schatz for helpful discussions and the Deutsche Forschungsgemeinschaft (SFB 513) for financial support.

- 
- [1] M. Albrecht, G. Hu, I. L. Guhr, T. C. Ulbrich, J. Boneberg, P. Leiderer, and G. Schatz, *Nature Materials* **4**, 203 (2005).
  - [2] A. M. Moser, K. Takano, D. T. Margulies, M. Albrecht, Y. Sonobe, Y. Ikeda, S. Sun, and E. E. Fullerton, *J. Phys. D* **35**, R157 (2002).
  - [3] N. Nakajima, T. Koide, T. Shidara, H. Miyauchi, H. Fukutani, A. Fujimori, K. Iio, T. Katayama, M. Nývlt, and Y. Suzuki, *Phys. Rev. Lett.* **81**, 5229 (1998).
  - [4] A. L. Shapiro, P. W. Rooney, M. Q. Tran, F. Hellman, K. M. Ring, K. L. Kavanagh, B. Rellinghaus, and D. Weller, *Phys. Rev. B* **60**, 12826 (1999).
  - [5] T. A. Tyson, S. D. Conradson, R. F. C. Farrow, and B. A. Jones, *Phys. Rev. B* **54**, R3702 (1996).
  - [6] J. O. Cross, M. Newville, F. Hellman, P. W. Rooney, A. L. Shapiro, and V. G. Harris, *J. Synchrotron Rad.* **8**, 880 (2001).
  - [7] M. Albrecht, A. Maier, F. Treubel, M. Maret, P. Poinso, and G. Schatz, *Europhys. Lett.* **56**, 884 (2001).
  - [8] K. Binder, *Phys. Rev. Lett.* **45**, 811 (1980).
  - [9] H. Berg and J. B. Cohen, *Metall. Trans.* **3**, 1797 (1972).
  - [10] Y. Gauthier, R. Baudoin-Savois, J. M. Bugnard, U. Bardi, and A. Atrei, *Surf. Sci.* **276**, 1 (1992).
  - [11] S. H. Yang, D. A. Drabold, J. B. Adams, P. Ordejón, and K. Glassford, *J. Phys.: Condens. Matter* **9**, L39 (1997).
  - [12] P. J. Feibelman, *Surf. Sci.* **423**, 169 (1999).
  - [13] P. Gambardella, M. Blanc, L. Burgi, K. Kuhnke, and K. Kern, *Surf. Sci.* **449**, 93 (2000).
  - [14] E. Lundgren, B. Stanka, W. Koprolin, M. Schmid, and P. Varga, *Surf. Sci.* **423**, 357 (1999).
  - [15] M. De Santis, R. Baudoin-Savois, P. Dolle, and M. C. Saint-Lager, *Phys. Rev. B* **66**, 085412 (2002).
  - [16] M. Albrecht, M. Maret, A. Maier, F. Treubel, B. Riedlinger, U. Mazur, G. Schatz, and S. Anders, *J. Appl. Phys.* **91**, 8153 (2002).
  - [17] M. T. Johnson, P. J. H. Bloemen, F. J. A. den Broeder, and J. J. de Vries, *Rep. Prog. Phys.* **59**, 1409 (1996).
  - [18] F. Menzinger and A. Paoletti, *Phys. Rev.* **143**, 365 (1966).